IEEE Access
Multidisciplinary | Rapid Review | Open Access Journal

Received 17 May 2022, accepted 6 June 2022, date of publication 16 June 2022, date of current version 26 July 2022.

Digital Object Identifier 10.1109/ACCESS.2022.3181693

Initial Orbit Determination Method for Low Earth Orbit Objects Using Too-Short Arc Based on Bistatic Radar

JINYE QU, DEFENG CHEN, HUAWEI CAO, TUO FU, AND SHUO ZHANG
School of Information and Electronics, Beijing Institute of Technology, Beijing 100081, China

Corresponding authors: Defeng Chen (defengchenbit@gmail.com) and Huawei Cao (hwei.cao@gmail.com)

This work was supported in part by the National Natural Science Foundation of China under Grant 62071041 and Grant 61701554; and in part by the Shanghai Aerospace and Technology Innovation Foundation, China, under Grant SAST-2020078.

ABSTRACT The problem of initial orbit determination (IOD) for Low Earth Orbit (LEO) objects using bistatic radar too-short arc (TSA) observations is addressed. For TSA observations, the traditional IOD methods suffer low accuracy. For LEO objects with stable attitude, the high order kinematic parameters can be obtained from the time derivatives of the radar echo phase. In this paper, an analytical IOD method is presented using bistatic radar TSA observations, which contain the position measurements (bistatic range, azimuth angle, and elevation angle) and the high order kinematic measurements (bistatic velocity, acceleration, and jerk). As the undetermined target state variables constitute a complex system of equations that can only be solved iteratively, an auxiliary coordinate system based on the bistatic geometry is defined to help reduce the equations to one unary quartic equation. Further, the closed-form expressions of the orbital state are derived. The performance of the proposed method is evaluated using linearization approximations. Numerical simulations are carried out for several typical LEO observation scenarios to demonstrate the performance of the proposed method.

INDEX TERMS Initial orbit determination, too-short arc, bistatic radar, root-mean-square error.

I. INTRODUCTION

With the development of space activities, the number of Low Earth Orbit (LEO) objects is increasing rapidly [1]. To maintain a catalogue of these LEO objects and detect new objects, the radar systems are widely used in space surveillance tasks. Because of the large number of objects and relatively limited sensors resources, a radar surveillance mode has been developed to improve the observing efficiency. Unlike in the traditional tracking mode, radar systems operating in the surveillance mode can produce a large number of too-short arc (TSA) observations, where the arc is usually several seconds [2]. When the detected object is new, the initial orbit determination (IOD) needs to be done to provide the basis for further data association and cataloguing [3], [4]. Using TSA observations, the classical IOD methods, such as the Laplace's, Gauss', or Double-r iteration, are unreliable and give poor results [5]. Therefore, it is highly important to develop a more accurate IOD method using TSAs.

The associate editor coordinating the review of this manuscript and approving it for publication was Fabrizio Santi.

The IOD problem has been studied extensively using TSA. The TSA measurements usually contain limited information to obtain a full orbit with valid accuracy, which is the intrinsic weakness of IOD problem [2]. Milani *et al.* developed a method using TSA angle and angle-rate measurements, and then the range and range rate were constrained to the admissible region [6]. The true orbit is obtained by searching parameters in the region. After identifying two TSAs from the same object, the orbit can be determined [7]. Based on the work of Milani, DeMars *et al.* proposed an IOD method using a discretization of the admissible region [8], and then developed a solution of IOD using Gaussian mixture models [9]. Ansalone and Hinagawa developed the method from optical data by exploiting genetic algorithms [10], [11]. They determined the optimal IOD solution by minimizing the observation errors. These methods apply to the angle-only measurements. As radars provide range information, the IOD method using two positions and the times, which is referred to as the Lambert problem, has been widely developed [12]–[14]. These methods are not applicable for TSAs. Tommei *et al.* developed the admissible region for radar data [15].

Considering the admissible region using radar observations, DeMars *et al.* applied it to the IOD from data association [16]. The methods solve the problem iteratively. The analytical method using three stations was proposed in [17]. However, the combination for three stations would increase the complexity of IOD process. The Herrick-Gibbs method used three position vectors and epochs to obtain the middle velocity vector. The method used the Taylor-series expansion to approximate the velocity [5]. Since the high accuracy doppler measurements can be obtained by the phase of radar echoes [18], IOD methods using doppler measurements were studied. Shang *et al.* proposed an IOD method using measurements from two stations in [19]. The method derived an analytical solution of IOD using the ranges, velocities, and accelerations from two stations simultaneously. Zhang *et al.* proposed a method using single-site higher order doppler measurements, where the radial acceleration and jerk are utilized [20]. Bistatic radars offer several advantages over monostatic radars, such as the configuration flexibility [21], [22]. Thus, developing an IOD method using bistatic radar is considered, and the crux of the problem is the complex relationship between the target state and doppler measurements.

In this paper, we propose a new IOD method based on bistatic radar TSA measurements. The method uses six measurements from a single arc observation to analytically determine the target state, where the bistatic range, azimuth and elevation angles are used for position determination, and the bistatic velocity, acceleration, and jerk are used for velocity determination. To solve the problem that the estimated parameters are coupling in a high order algebraic system, a new coordinate system is defined for decoupling, and finally the analytical expression is derived by coordinate transformation. The RMSE (root-mean-square error) is used to evaluate the IOD performance, and singular cases with low accuracy of velocity determination are considered.

This paper is organized as follows. Section II introduces the bistatic observation model and the relationship between observations and the object state, then the IOD method is presented by solving the equations formed by the measurements and state, including position determination and velocity determination. Section III presents the linearized error analysis using the RMSE to evaluate the performance of IOD. Section IV presents Monte Carlo simulations and the comparison between the theoretical result and the simulation result. Observation scenarios of typical LEO objects are considered. Some singular cases are discussed to avoid bad IOD performance. Finally, Section V concludes the paper.

II. IOD METHOD

A. OBSERVATION MODEL

The orbital state is described in the Earth-centered Inertial (ECI) system. Let the position vector be $\vec{\mathbf{r}}$ and the velocity vector be $\vec{\mathbf{v}}$. Let $\vec{\mathbf{X}} = \left[\vec{\mathbf{r}}^T, \vec{\mathbf{v}}^T\right]^T$ denote the state vector. As shown in Figure 1, the two stations are located at S_t and S_r, and the station position vectors are $\vec{\mathbf{S}}_t$ and $\vec{\mathbf{S}}_r$, respectively. The target is located at P, and S_tS_rP forms the bistatic plane. To simplify the analysis, the Earth is regarded as an ideal sphere. In the absence of perturbations, the target motion is regarded as the two-body problem. For a single short arc observation, the station is assumed to be fixed, while the station velocity, acceleration, and jerk caused by the Earth's rotation are included.

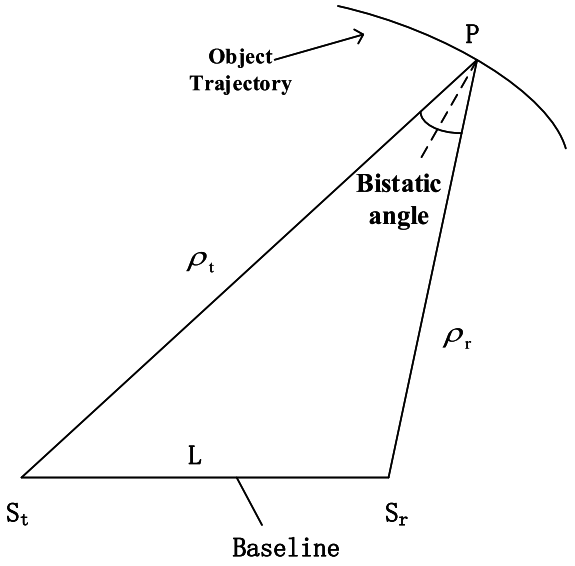

FIGURE 1. Bistatic radar geometry.

For a single short arc, the bistatic radar produces six measurements, which are designated the observation vector $\vec{\mathbf{Y}} = \left[\rho, az, el, \dot{\rho}, \ddot{\rho}, \dddot{\rho}\right]^T$, where ρ is the bistatic range. Based on the receiving station, the topocentric coordinate system (SEZ) can be established. Then, the angle measurements az and el are defined in the SEZ system. $\dot{\rho}$, $\ddot{\rho}$, and $\dddot{\rho}$ are the bistatic velocity, acceleration, and jerk, respectively.

The bistatic range ρ is the sum of the bistatic transmitter-to-target range ρ_t and the bistatic receiver-to-target range ρ_r:

$$\rho = \rho_{\mathrm{t}} + \rho_{\mathrm{r}} = \sqrt{\left(\vec{\mathrm{r}} - \vec{\mathbf{S}}_{\mathrm{t}}\right)^2} + \sqrt{\left(\vec{\mathrm{r}} - \vec{\mathbf{S}}_{\mathrm{r}}\right)^2} \tag{1}$$

The SEZ system is defined in [23] and shown in Figure 2, where the origin is located at the receiving station, the S-axis points the South, the E-axis points the East, and SEZ composes a right-hand coordinate system. The azimuth (az) is the angle measured from north, clockwise to the location beneath the object, and the elevation (el) is measured from the local horizon positive up to the object. Hence, the angle measurements are:

$$\begin{aligned} az &= \arctan\left(-\frac{\rho_{\mathrm{E}}}{\rho_S}\right) \\ el &= arctan\left(\frac{\rho_Z}{\sqrt{\rho_S^2 + \rho_E^2}}\right) \end{aligned} \tag{2}$$

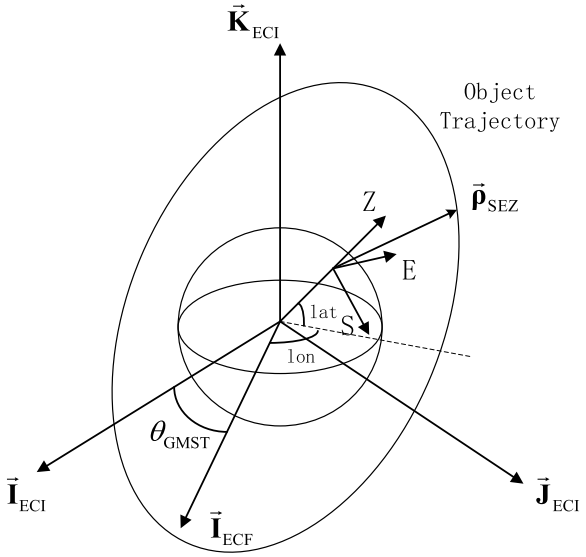

FIGURE 2. Topocentric-horizon coordinate system (SEZ).

The azimuth angle is usually reconciled to range from 0 to 360°, and the value of elevation angle usually ranges from 0 to 90°.

The bistatic velocity $\dot{\rho}$ is defined as the sum of the two velocities of the target relative to the two stations, and the acceleration and jerk are obtained by differentiating kinematic measurements with respect to time:

$$\begin{aligned}\dot{\rho} &= \frac{d\rho}{dt} = \dot{\rho}_r + \dot{\rho}_t \\ \ddot{\rho} &= \frac{d\dot{\rho}}{dt} = \ddot{\rho}_r + \ddot{\rho}_t \\ \dddot{\rho} &= \frac{d\ddot{\rho}}{dt} = \dddot{\rho}_r + \dddot{\rho}_t\end{aligned} \tag{3}$$

To establish the observation equations of the high order kinematic measurements, the method of obtaining the measurements is considered. The bistatic velocity, acceleration, and jerk can be estimated from the phase of radar echoes. Assuming that the radar system uses the single carrier frequency coherent pulse train, the transmitted coherent pulse train can be expressed as

$$s_t(t) = \sum_{n=1}^{N} p_t\left(t - nT_p\right) \exp\left(j2\pi f_c t\right) \tag{4}$$

where N is the number of the pulses, T_p is the pulse repetition period, f_c is the carrier frequency, and p_t is the waveform function of the pulse. The received baseband signal is:

$$s_r(t) = \sum_{n=1}^{N} p_t\left(t - nT_p - \tau_n\right) \exp\left(j2\pi f_c \tau_n\right) + w(t) \tag{5}$$

where $w(t)$ is the additive white Gaussian noise, and τ_n is the time delay. τ_n is related to the bistatic range:

$$\tau_n = \frac{\rho_r\left(nT_p\right) + \rho_t\left(nT_p\right)}{c} \tag{6}$$

where c is the speed of light. The relative ranges are modelled as a polynomial. Let t_0 denote the reference time and $\Delta t = t - t_0$ denote the relative time. The relative range can be described as:

$$\rho_r(t) = \rho_{r0} + \dot{\rho}_r \Delta t + \frac{1}{2}\ddot{\rho}_r \Delta t^2 + \frac{1}{6}\dddot{\rho}_r \Delta t^3 + \cdots \tag{7a}$$

$$\rho_t(t) = \rho_{t0} + \dot{\rho}_t \Delta t + \frac{1}{2}\ddot{\rho}_t \Delta t^2 + \frac{1}{6}\dddot{\rho}_t \Delta t^3 + \cdots \tag{7b}$$

In the case of short arc observations, the target motion is approximately a third-order polynomial. Then, the bistatic doppler measurements can be derived as:

$$\rho(t) \approx \rho_0 + \dot{\rho}\Delta t + \frac{1}{2}\ddot{\rho}\Delta t^2 + \frac{1}{6}\dddot{\rho}\Delta t^3 \tag{8}$$

The maximum likelihood (ML) estimation is used to extract the coefficients in the equation. As the range is usually derived from the time delay, only the three high order kinematic measurements are obtained by the ML estimation. Let θ denote the estimated parameter vector. The ML estimator can be obtained as:

$$\hat{\theta} = \arg\max_{\theta} pdf\left(\mathbf{s}_r, \theta\right) \tag{9}$$

where $\mathbf{s}_r$ is the discrete-time signal sampled from the baseband received signal. The three high order kinematic measurements can be estimated from the estimation process. In practice, most of radars use the linear frequency modulated (LFM) pulse train for space surveillance. The errors of measurements are analyzed based on the results of references [18]. When the reference time t_0 is the middle time of the integration time interval, the CRLB of the high order kinematic measurements are derived in [24].

In fact, the measurement vector $\vec{\mathbf{Y}}$ can be considered to be obtained from the instantaneous state $\left[\vec{\mathbf{r}}_0^T, \vec{\mathbf{v}}_0^T\right]^T$ at the reference time t_0. For simplicity, the subscripts are omitted. As the bistatic high order kinematic measurements are the sum of those relative to both stations, without loss of generality, the terms of the target relative to the receiving station are considered. The velocity can be formulated in the ECI system:

$$\dot{\rho}_r = \frac{\vec{\boldsymbol{\rho}}_r \cdot \left(\vec{\mathbf{v}} - \dot{\vec{\mathbf{S}}}_r\right)}{\rho_r} \tag{10}$$

where $\vec{\boldsymbol{\rho}}_r$ is the relative vector from the station to the target, and $\dot{\vec{\mathbf{S}}}_r$ is the velocity vector of receiving station caused by the Earth's rotation. The acceleration $\ddot{\rho}_r$ can be generated by differentiating $\dot{\rho}_r$ with respect to time:

$$\ddot{\rho}_r = \frac{1}{\rho_r}\left(\left(\vec{\mathbf{v}} - \dot{\vec{\mathbf{S}}}_r\right)^2 - \dot{\rho}_r^2\right) + \frac{\left(\ddot{\vec{\mathbf{r}}} - \ddot{\vec{\mathbf{S}}}_r\right) \cdot \vec{\boldsymbol{\rho}}_r}{\rho_r} \tag{11}$$

where v is the norm of $\vec{\mathbf{v}}$, and $\ddot{\vec{\mathbf{r}}}$ is the acceleration vector of the target in the two-body model. $\ddot{\vec{\mathbf{S}}}_r$ is the acceleration vector of

receiving station caused by the Earth's rotation. The motion vectors $\ddot{\vec{\mathbf{r}}}$ and $\dddot{\vec{\mathbf{r}}}$ can be derived from the target state:

$$\begin{aligned}\ddot{\vec{\mathbf{r}}} &= -\frac{\mu}{r^3}\vec{\mathbf{r}} \\ \dddot{\vec{\mathbf{r}}} &= -\frac{\mu}{r^3}\vec{\mathbf{v}} + 3\mu\frac{\vec{\mathbf{r}}\cdot\vec{\mathbf{v}}}{r^5}\vec{\mathbf{r}}\end{aligned} \tag{12}$$

where r is the norm of $\vec{\mathbf{r}}$ and μ is the gravitational parameter of the Earth. Since the jerk vector of the target can be represented by the position vector $\vec{\mathbf{r}}$ and the velocity vector $\vec{\mathbf{v}}$, the jerk $\dddot{\rho}_r$ can be expressed as follows:

$$\dddot{\rho}_r = -\frac{3\dot{\rho}_r\ddot{\rho}_r}{\rho_r} + \frac{3\left(\vec{v}-\dot{\vec{\mathbf{S}}}_r\right)\cdot\left(\ddot{\vec{\mathbf{r}}}-\ddot{\vec{\mathbf{S}}}_r\right)}{\rho_r} + \frac{\left(\dddot{\vec{\mathbf{r}}}-\dddot{\vec{\mathbf{S}}}_r\right)\cdot\vec{\rho}_r}{\rho_r} \tag{13}$$

where $\dddot{\vec{\mathbf{S}}}_r$ the jerk vector of receiving station caused by the Earth's rotation. Similarly, the terms relative to the transmitting station can also be formulated.

B. IOD PROCESS

The target position vector can be obtained using three position measurements, $[\rho, az, el]$. According to the relationship between the SEZ system and the measurements, a transformation is performed to yield

$$\vec{\boldsymbol{\rho}}_{\mathrm{SEZ}} = \begin{bmatrix} -\rho_{\mathrm{r}}\cos(el)\cos(az) \\ \rho_{\mathrm{r}}\cos(el)\sin(az) \\ \rho_{\mathrm{r}}\sin(el) \end{bmatrix} \tag{14}$$

The bistatic receiver-to-target range ρ_{r}, according to the geometry of bistatic stations and the target, can be written as:

$$\rho_{\mathrm{r}} = \frac{\rho^2 - L^2}{2(\rho - L\cos(\theta))} \tag{15}$$

where L is the baseline range, and θ is the angle between the vectors $\overrightarrow{\mathrm{S_rP}}$ and $\overrightarrow{\mathrm{S_rS_t}}$. Let $\vec{\mathbf{e}}_{LOS}$ represent the unit vector of the line-of-sight (LOS) direction, which is written as:

$$\vec{\mathbf{e}}_{LOS} = \begin{bmatrix} -\cos(el)\cos(az) \\ \cos(el)\sin(az) \\ \sin(el) \end{bmatrix} \tag{16}$$

Finally, the position state of the target in ECI can be expressed by:

$$\vec{\mathbf{r}} = \mathbf{M}_{\mathrm{ECI}\leftarrow\mathrm{ECF}}\cdot\mathbf{M}_{\mathrm{ECF}\leftarrow\mathrm{SEZ}}\cdot\vec{\boldsymbol{\rho}}_{\mathrm{SEZ}} + \vec{\mathbf{S}}_{\mathrm{r}} \tag{17}$$

where the transformation matrices are provided in [23]. Note that $\mathbf{M}_{\mathrm{ECF}\leftarrow\mathrm{SEZ}}$ depends only on the latitude and longitude of the receiving station.

To get the velocity vector, the three high order kinematic measurements are required. The three equations in Equation (3) are used to solve the three velocity components in the ECI system. Compared with the monostatic radar, the bistatic radar produces a measured velocity $\dot{\rho}$ that is combined by the velocities relative to both stations, and the velocity of the target relative to a single station is unknown. Therefore, the three velocity components in the ECI system

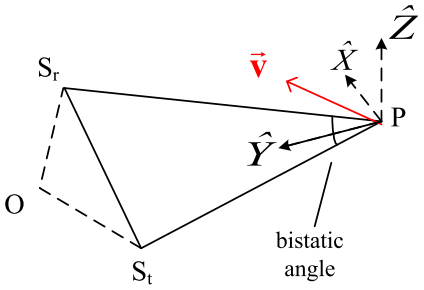

FIGURE 3. Coordinate system for velocity determination.

are coupled in three equations of Equation (3), which is not feasible to directly calculate an analytical solution. Thus, an auxiliary coordinate system $\hat{X}\hat{Y}\hat{Z}$ is considered as shown in Figure 3, where the origin coincides with the target and the axes $\hat{X}$ and $\hat{Y}$ lie in the bistatic plane. Axis $\hat{Y}$ is collinear with the bisector of the bistatic angle, axis $\hat{Z}$ is vertical to the bistatic plane, and $\hat{X}\hat{Y}\hat{Z}$ composes a right-hand coordinate system. The unit vectors of this system are obtained:

$$\vec{\mathbf{e}}_{\hat{Y}} = -\frac{\frac{\vec{\rho}_{\mathrm{r}}}{\rho_{\mathrm{r}}}+\frac{\vec{\rho}_{\mathrm{t}}}{\rho_{\mathrm{t}}}}{\left|\frac{\vec{\rho}_{\mathrm{r}}}{\rho_{\mathrm{r}}}+\frac{\vec{\rho}_{\mathrm{t}}}{\rho_{\mathrm{t}}}\right|}, \vec{\mathbf{e}}_{\hat{Z}} = \frac{\vec{\boldsymbol{\rho}}_{\mathrm{r}}\times\vec{\boldsymbol{\rho}}_{\mathrm{t}}}{\left|\vec{\boldsymbol{\rho}}_{\mathrm{r}}\times\vec{\boldsymbol{\rho}}_{\mathrm{t}}\right|}, \vec{\mathbf{e}}_{\hat{X}} = \vec{\mathbf{e}}_{\hat{Y}}\times\vec{\mathbf{e}}_{\hat{Z}} \tag{18}$$

The transformation matrices between the ECI system and $\hat{X}\hat{Y}\hat{Z}$ system are:

$$\begin{aligned}\mathbf{M}_{\mathrm{ECI}\leftarrow\hat{X}\hat{Y}\hat{Z}} &= \left[\vec{\mathbf{e}}_{\hat{X}}, \vec{\mathbf{e}}_{\hat{Y}}, \vec{\mathbf{e}}_{\hat{Z}}\right] \\ \mathbf{M}_{\hat{X}\hat{Y}\hat{Z}\leftarrow\mathrm{ECI}} &= \mathbf{M}^T_{\mathrm{ECI}\leftarrow\hat{X}\hat{Y}\hat{Z}}\end{aligned} \tag{19}$$

The stations lie in the bistatic plane, which means that the position vectors between stations and the target can be described in this system:

$$\begin{aligned}\hat{\vec{\rho}}_{\mathrm{r}} &= \mathbf{M}_{\hat{X}\hat{Y}\hat{Z}\leftarrow\mathrm{ECI}}\cdot\hat{\vec{\rho}}_{\mathrm{r}} = \hat{x}_{\mathrm{r}}\vec{\mathbf{e}}_{\hat{X}} + \hat{y}_{\mathrm{r}}\vec{\mathbf{e}}_{\hat{Y}} \\ \hat{\vec{\rho}}_{\mathrm{t}} &= \mathbf{M}_{\hat{X}\hat{Y}\hat{Z}\leftarrow\mathrm{ECI}}\cdot\hat{\vec{\rho}}_{\mathrm{t}} = \hat{x}_{\mathrm{t}}\vec{\mathbf{e}}_{\hat{X}} + \hat{y}_{\mathrm{t}}\vec{\mathbf{e}}_{\hat{Y}}\end{aligned} \tag{20}$$

Based on the fact that $\vec{\mathbf{e}}_{\hat{Y}}$ is collinear with the bisector, according to the angular bisector properties, the coefficients of (20) have the following relationship:

$$\left|\frac{\hat{x}_{\mathrm{r}}}{\hat{y}_{\mathrm{r}}}\right| = \left|\frac{\hat{x}_{\mathrm{t}}}{\hat{y}_{\mathrm{t}}}\right| \tag{21}$$

Because the position vector has been determined, the components in Equation (20) can be calculated. The velocity vector is described in $\hat{X}\hat{Y}\hat{Z}$ system as

$$\hat{\vec{\mathbf{v}}} = \left(v_{\hat{x}}, v_{\hat{y}}, v_{\hat{z}}\right)^T = \mathbf{M}_{\hat{X}\hat{Y}\hat{Z}\leftarrow\mathrm{ECI}}\cdot\vec{\mathbf{v}} \tag{22}$$

Combining the definitions of the $\hat{X}\hat{Y}\hat{Z}$ system and the expression of $\dot{\rho}$ in Equations (3) and (10), $v_{\hat{y}}$ can be derived as:

$$v_{\hat{y}} = \frac{\dot{\rho} + \left(\vec{\boldsymbol{\rho}}_{\mathrm{r}}\cdot\dot{\vec{\mathbf{S}}}_{\mathrm{r}}\right)/\rho_{\mathrm{r}} + \left(\vec{\boldsymbol{\rho}}_{\mathrm{t}}\cdot\dot{\vec{\mathbf{S}}}_{\mathrm{t}}\right)/\rho_{\mathrm{t}}}{\left|\frac{\vec{\rho}_{\mathrm{r}}}{\rho_{\mathrm{r}}}+\frac{\vec{\rho}_{\mathrm{t}}}{\rho_{\mathrm{t}}}\right|} \tag{23}$$

Therefore, the components $v_{\hat{x}}$ and $v_{\hat{z}}$ are solutions to the second and third equations of (3). To solve this problem,

the high order doppler measurements are described in the $\hat{X}\hat{Y}\hat{Z}$ system. Let $\dot{\hat{\vec{S}}}_{\mathbf{r}} = \left[v_{\mathrm{rx}}, v_{\mathrm{ry}}, v_{\mathrm{rz}}\right]^T$ and $\dot{\hat{\vec{S}}}_{\mathbf{t}} = \left[v_{\mathrm{tx}}, v_{\mathrm{ty}}, v_{\mathrm{tz}}\right]^T$ denote the coordinates of station velocities in the $\hat{X}\hat{Y}\hat{Z}$ system. The bistatic velocity $\dot{\rho}$ equals $\dot{\rho}_{\mathrm{r}} + \dot{\rho}_{\mathrm{t}}$, where

$$\dot{\rho}_{\mathrm{r}} = \hat{\vec{\mathbf{v}}} \cdot \frac{\hat{\vec{\boldsymbol{\rho}}}_{\mathrm{r}}}{\rho_{\mathrm{r}}} - \frac{\hat{\vec{\boldsymbol{\rho}}}_{\mathrm{r}} \cdot \dot{\hat{\vec{\mathbf{S}}}}_{\mathrm{r}}}{\rho_{\mathrm{r}}} = \frac{x_{\mathrm{r}}}{\rho_{\mathrm{r}}} v_{\hat{x}} + \frac{y_{\mathrm{r}}}{\rho_{\mathrm{r}}} v_{\hat{y}} - \frac{\hat{\vec{\boldsymbol{\rho}}}_{\mathrm{r}} \cdot \dot{\hat{\vec{\mathbf{S}}}}_{\mathrm{r}}}{\rho_{\mathrm{r}}} \tag{24a}$$

$$\dot{\rho}_{\mathrm{t}} = \hat{\vec{\mathbf{v}}} \cdot \frac{\hat{\vec{\boldsymbol{\rho}}}_{\mathrm{t}}}{\rho_{\mathrm{t}}} - \frac{\hat{\vec{\boldsymbol{\rho}}}_{\mathrm{t}} \cdot \dot{\hat{\vec{\mathbf{S}}}}_{\mathrm{t}}}{\rho_{\mathrm{t}}} = \frac{x_{\mathrm{t}}}{\rho_{\mathrm{t}}} v_{\hat{x}} + \frac{y_{\mathrm{t}}}{\rho_{\mathrm{t}}} v_{\hat{y}} - \frac{\hat{\vec{\boldsymbol{\rho}}}_{\mathrm{t}} \cdot \dot{\hat{\vec{\mathbf{S}}}}_{\mathrm{t}}}{\rho_{\mathrm{t}}} \tag{24b}$$

After substituting Equation (24) into Equation (3), the acceleration can be obtained:

$$\begin{aligned}
\ddot{\rho}_{\mathrm{r}} = {} & \frac{1}{\rho_{\mathrm{r}}}\left((v_{\hat{x}} - v_{\mathrm{rx}})^2 + (v_{\hat{y}} - v_{\mathrm{ry}})^2 + (v_{\hat{z}} - v_{\mathrm{rz}})^2\right) \\
& - \frac{1}{\rho_{\mathrm{r}}}\left(\frac{x_{\mathrm{r}}}{\rho_{\mathrm{r}}} v_{\hat{x}} + \frac{y_{\mathrm{r}}}{\rho_{\mathrm{r}}} v_{\hat{y}} - \frac{\hat{\vec{\boldsymbol{\rho}}}_{\mathrm{r}} \cdot \dot{\hat{\vec{\mathbf{S}}}}_{\mathrm{r}}}{\rho_{\mathrm{r}}}\right)^2 + \frac{\left(\ddot{\vec{\mathbf{r}}} - \ddot{\hat{\vec{\mathbf{S}}}}_{\mathrm{r}}\right) \cdot \vec{\boldsymbol{\rho}}_{\mathrm{r}}}{\rho_{\mathrm{r}}} \\
\ddot{\rho}_{\mathrm{t}} = {} & \frac{1}{\rho_{\mathrm{t}}}\left((v_{\hat{x}} - v_{\mathrm{tx}})^2 + (v_{\hat{y}} - v_{\mathrm{ty}})^2 + (v_{\hat{z}} - v_{\mathrm{tz}})^2\right) \\
& - \frac{1}{\rho_{\mathrm{t}}}\left(\frac{x_{\mathrm{t}}}{\rho_{\mathrm{t}}} v_{\hat{x}} + \frac{y_{\mathrm{t}}}{\rho_{\mathrm{t}}} v_{\hat{y}} - \frac{\hat{\vec{\boldsymbol{\rho}}}_{\mathrm{t}} \cdot \dot{\hat{\vec{\mathbf{S}}}}_{\mathrm{t}}}{\rho_{\mathrm{t}}}\right)^2 + \frac{\left(\ddot{\vec{\mathbf{r}}} - \ddot{\hat{\vec{\mathbf{S}}}}_{\mathrm{t}}\right) \cdot \vec{\boldsymbol{\rho}}_{\mathrm{t}}}{\rho_{\mathrm{t}}}
\end{aligned} \tag{25}$$

To simplify the form, a substitution for the coefficients in former equations is done. The specific substitution is provided in Appendix A. Then the single velocity expressed in Equation (25) is simplified as:

$$\begin{aligned}
\ddot{\rho}_{\mathrm{r}} &= k_{\mathrm{r}1} v_{\hat{x}}^2 + k_{\mathrm{r}2} v_{\hat{x}} + l_{\mathrm{r}1} v_{\hat{z}}^2 + l_{\mathrm{r}2} v_{\hat{z}} + m_{\mathrm{r}} \\
\ddot{\rho}_{\mathrm{t}} &= k_{\mathrm{t}1} v_{\hat{x}}^2 + k_{\mathrm{t}2} v_{\hat{x}} + l_{\mathrm{t}1} v_{\hat{z}}^2 + l_{\mathrm{t}2} v_{\hat{z}} + m_{\mathrm{t}}
\end{aligned} \tag{26}$$

Considering that the bistatic acceleration $\ddot{\rho}$ equals $\ddot{\rho}_{\mathrm{r}} + \ddot{\rho}_{\mathrm{t}}$, a further substitution is formed:

$$\begin{aligned}
k_1 &= k_{\mathrm{t}1} + k_{\mathrm{r}1}, k_2 = k_{\mathrm{t}2} + k_{\mathrm{r}2} \\
l_1 &= l_{\mathrm{t}1} + l_{\mathrm{r}1}, l_2 = l_{\mathrm{t}1} + l_{\mathrm{r}1} \\
m_1 &= m_{\mathrm{t}} + m_{\mathrm{r}}
\end{aligned} \tag{27}$$

Then $\ddot{\rho}$ can be expressed as:

$$\ddot{\rho} = k_1 v_{\hat{x}}^2 + k_2 v_{\hat{x}} + l_1 v_{\hat{z}}^2 + l_2 v_{\hat{z}} + m_1 \tag{28}$$

To separate the two unknowns, a further variable substitution is made:

$$v'_{\hat{z}} = v_{\hat{z}} + \frac{l_2}{2l_1} \tag{29a}$$

$$m'_1 = m_1 - \frac{l_2^2}{4l_1} \tag{29b}$$

Then (28) can be expressed as:

$$\ddot{\rho} = k_1 v_{\hat{x}}^2 + k_2 v_{\hat{x}} + l_1 v'^2_{\hat{z}} + m'_1 \tag{30}$$

The two unknowns can be separated, and $v'_{\hat{z}}$ can be written by $v_{\hat{x}}$:

$$v'_{\hat{z}} = \pm\sqrt{-\frac{k_1 v_{\hat{x}}^2 + k_2 v_{\hat{x}} + m'_1 - \ddot{\rho}}{l_1}} \tag{31}$$

Similarly, substituting Equations (24) and (25) into Equation (3), the bistatic jerk $\dddot{\rho}$ can be simplified and expressed as a binary cubic equation of $v_{\hat{x}}$ and $v_{\hat{z}}$:

$$\begin{aligned}
\dddot{\rho} = {} & c_1 v_{\hat{x}}^3 + c_2 v_{\hat{x}}^2 + c_3 v_{\hat{x}} + c_4 v_{\hat{x}} v_{\hat{z}}^2 \\
& + c_5 v_{\hat{z}}^2 + c_6 v_{\hat{z}} + c_7 + c_8 v_{\hat{x}} v_{\hat{z}}
\end{aligned} \tag{32}$$

Then $v'_{\hat{z}}$ is used to replace $v_{\hat{z}}$ and (32) is updated as:

$$\begin{aligned}
\dddot{\rho} = {} & c_1 v_{\hat{x}}^3 + c_2 v_{\hat{x}}^2 + c'_3 v_{\hat{x}} + c_4 v_{\hat{x}} v'^2_{\hat{z}} \\
& + c_5 v'^2_{\hat{z}} + c'_6 v'_{\hat{z}} + c'_7 + c'_8 v_{\hat{x}} v'_{\hat{z}}
\end{aligned} \tag{33}$$

The specific substitution is provided in Appendix V. Let m_2 equal $m'_1 - \ddot{\rho}$. Combining with (30), an equation of $v_{\hat{x}}$ is obtained:

$$\begin{aligned}
\dddot{\rho} = {} & c_1 v_{\hat{x}}^3 + c_2 v_{\hat{x}}^2 + c'_3 v_{\hat{x}} + c'_7 \\
& - (c_4 v_{\hat{x}} + c_5)\left(\frac{k_1 v_{\hat{x}}^2 + k_2 v_{\hat{x}} + m_2}{l_1}\right) \\
& \pm (c'_6 + c'_8 v_{\hat{x}})\sqrt{-\frac{k_1 v_{\hat{x}}^2 + k_2 v_{\hat{x}} + m_2}{l_1}}
\end{aligned} \tag{34}$$

According to the angular bisector properties shown in Equation (21), the coefficient of the highest term $v_{\hat{x}}^3$ in Equation (34), which is $c_1 - \frac{c_4 k_1}{l_1}$, equals 0. Therefore, Equation (34) can be simplified into a quartic equation of $v_{\hat{x}}$:

$$f_1 v_{\hat{x}}^4 + f_2 v_{\hat{x}}^3 + f_3 v_{\hat{x}}^2 + f_4 v_{\hat{x}} + f_5 = 0 \tag{35}$$

Additionally, the specific substitution is provided in Appendix V. To solve Equation (35), the method for finding roots for quartic equations, which is provided in Appendix V. After finding $v_{\hat{x}}$, $v_{\hat{z}}$ can be derived using (31). Noticing that there exist two ambiguity solutions, the unique solution can be determined by combining with (32). Once the velocity in the $\hat{X}\hat{Y}\hat{Z}$ system is expressed, the velocity vector $\vec{\mathbf{v}}$ can be calculated by using the transformation matrix shown in (19).

Regardless of the measured error, the system of equations could produce four complex values of $v_{\hat{x}}$, which lead to four sets of $\hat{\vec{\mathbf{v}}}$, and there is at least one real set that matches the true value of target state. All these sets of solutions meet the existing conditions, and some additional information could be used to solve this problem. The measured rate of angle can be used, but in order to pursue better orbit determination accuracy, it is not used for deriving the analytical expression. In actual observation scenarios, due to the disturbance of the measured error, the equation (35) will produce at most four complex solutions, which means that the unique true value solution may have an non-zero imaginary part. In this case, the imaginary part of the unique root is discarded and the error between the real part and the true value are considered.

In summary, by using six measurements acquired from a single TSA bistatic radar observation, an analytical expression of the target state is obtained.

III. ERROR ANALYSIS

To analyze the performance of the proposed IOD method, the covariance matrix of the target state is required. As the transition from the target state to radar observation is nonlinear, the state estimate covariance does not have a compact analytical expression. The linearization method is used to approximately generate the covariance. Let $\mathbf{C_X}$ denote the state covariance matrix and $\mathbf{C_Y}$ denote the observation covariance matrix. According to the principle of the linearization method, $\mathbf{C_X}$ can be derived as:

$$\mathbf{C_X} = \frac{\partial \vec{\mathbf{X}}}{\partial \vec{\mathbf{Y}}^T} \cdot \mathbf{C_Y} \cdot \frac{\partial \vec{\mathbf{X}}^T}{\partial \vec{\mathbf{Y}}} \tag{36}$$

The root-mean-square error is frequently used to express the differences between the observed values and the estimated values. The initial orbit can be regarded as the estimated state derived from the radar observations. Hence, we define the position root-mean-square error (PRMSE) and the velocity root-mean-square error (VRMSE) to represent the position accuracy and the velocity accuracy [25]. They can be generated as:

$$\begin{aligned} \text{PRMSE} &= \sqrt{\mathbf{C_X}(1,1) + \mathbf{C_X}(2,2) + \mathbf{C_X}(3,3)} \\ \text{VRMSE} &= \sqrt{\mathbf{C_X}(4,4) + \mathbf{C_X}(5,5) + \mathbf{C_X}(6,6)} \end{aligned} \tag{37}$$

To simplify the analysis, the covariance matrix is derived under the assumption of the two-body motion model, where the oblateness is neglected. Suppose that the measurements from the receiving station are disturbed only by random noise, which means that the system errors caused by sensors are removed. Let $\left[\sigma_\rho, \sigma_{az}, \sigma_{el}, \sigma_{\dot\rho}, \sigma_{\ddot\rho}, \sigma_{\dddot\rho}\right]$ represent the standard deviations of the six measurements.

Considering the observation covariance matrix, some studies for LFM signal radar measurements have been done in [18] and [24]. According to the IOD process shown in Sec. II, the six measurements can be regarded as two measurement groups: the position measurements $[\rho, az, el]$, and the kinematic measurements $\left[\dot\rho, \ddot\rho, \dddot\rho\right]$. The two groups are assumed to be mutually independent. Then the covariance matrix can be regarded as consisting of two submatrices: the covariance matrix of position measurements $\mathbf{C}_{position}$, and the covariance matrix of kinematic measurements $\mathbf{C}_{doppler}$. The matrix can be written as:

$$\mathbf{C_Y} = \begin{bmatrix} \mathbf{C}_{position} & \mathbf{0} \\ \mathbf{0} & \mathbf{C}_{doppler} \end{bmatrix} \tag{38}$$

where $\mathbf{C}_{position}$ is a diagonal matrix of measurement variances. The high order kinematic measurements are estimated by the maximum likelihood method using the high precision phase characteristic from radar echoes. The covariance matrix $\mathbf{C}_{doppler}$ is the inverse of the Fisher information matrix.

A. POSITION ROOT-MEAN-SQUARE ERROR (PRMSE)

Let $\mathbf{C}^{\text{pos}}_{\text{ECI}}$ denote the covariance matrix of the position vector in ECI system, and $\mathbf{C}^{\text{pos}}_{\text{SEZ}}$ denote that in the SEZ system. As the transformation matrix is provided in [25], $\mathbf{C}^{\text{pos}}_{\text{ECI}}$ can be obtained:

$$\mathbf{C}^{\text{pos}}_{\text{ECI}} = \mathbf{M}_{\text{ECI}\leftarrow\text{SEZ}} \cdot \mathbf{C}^{\text{pos}}_{\text{SEZ}} \cdot \mathbf{M}^T_{\text{ECI}\leftarrow\text{SEZ}} \tag{39}$$

Since $\mathbf{M}_{\text{ECI}\leftarrow\text{SEZ}}$ is related to the Local Sidereal Time (LST), the station longitude, and the station latitude, it is orthogonal with no relationship with measurements. The PRMSE is the square root of the trace of $\mathbf{C}^{\text{pos}}_{\text{ECI}}$, which equals the trace of $\mathbf{C}^{\text{pos}}_{\text{SEZ}}$. Let $\vec{\mathbf{Y}}_{\text{pos}} = [\rho, az, el]^T$ denote the observation vector that is used for position determination. Then $\mathbf{C}^{\text{pos}}_{\text{SEZ}}$ can be derived using linearization approach:

$$\mathbf{C}^{\text{pos}}_{\text{SEZ}} = \frac{\partial \vec{\boldsymbol{\rho}}_{\text{SEZ}}}{\partial \vec{\mathbf{Y}}^T_{\text{pos}}} \cdot \mathbf{C}_{position} \cdot \frac{\partial \vec{\boldsymbol{\rho}}^T_{\text{SEZ}}}{\partial \vec{\mathbf{Y}}_{\text{pos}}} \tag{40}$$

Based on the chain rule, the partial derivatives can be written as:

$$\begin{aligned} \frac{\partial \vec{\boldsymbol{\rho}}_{\text{SEZ}}}{\partial \rho} &= \frac{\partial \rho_{\text{r}}}{\partial \rho} \cdot \vec{\mathbf{e}}_{LOS} \\ \frac{\partial \vec{\boldsymbol{\rho}}_{\text{SEZ}}}{\partial az} &= \rho_{\text{r}} \cdot \frac{\partial \vec{\mathbf{e}}_{LOS}}{\partial az} + \frac{\partial \rho_{\text{r}}}{\partial (\cos(\theta))} \cdot \frac{\partial (\cos(\theta))}{\partial az} \cdot \vec{\mathbf{e}}_{LOS} \\ \frac{\partial \vec{\boldsymbol{\rho}}_{\text{SEZ}}}{\partial el} &= \rho_{\text{r}} \cdot \frac{\partial \vec{\mathbf{e}}_{LOS}}{\partial el} + \frac{\partial \rho_{\text{r}}}{\partial (\cos(\theta))} \cdot \frac{\partial (\cos(\theta))}{\partial el} \cdot \vec{\mathbf{e}}_{LOS} \end{aligned} \tag{41}$$

where $\cos(\theta) = \left(\overrightarrow{\text{S}_\text{r}\text{S}_\text{t}} \cdot \vec{\mathbf{e}}_{LOS}\right)/L$. Let C_θ represent $\cos(\theta)$ for simplicity. Other terms can be derived using derivative rules. After substituting Equation (41) into Equation (40) and using Equation (37), the PRMSE can be obtained:

$$\text{PRMSE} = \sqrt{\begin{pmatrix} \left(\frac{\partial \rho_{\text{r}}}{\partial \rho}\right)^2 \sigma_\rho^2 + \left(\rho_{\text{r}}^2 + \left(\frac{\partial \rho_{\text{r}}}{\partial C_\theta}\frac{\partial C_\theta}{\partial el}\right)^2\right)\sigma_{el}^2 \\ + \left(\rho_{\text{r}}^2 \cos^2(el) + \left(\frac{\partial \rho_{\text{r}}}{\partial C_\theta}\frac{\partial C_\theta}{\partial az}\right)^2\right)\sigma_{az}^2 \end{pmatrix}} \tag{42}$$

B. VELOCITY ROOT-MEAN-SQUARE ERROR (VRMSE)

Similarly, let $\mathbf{C}^{\text{vel}}_{\text{ECI}}$ denote the covariance matrix of the velocity vector in the ECI system. The VRMSE is the square root of the trace of $\mathbf{C}^{\text{vel}}_{\text{ECI}}$, which is derived by:

$$\mathbf{C}^{\text{vel}}_{\text{ECI}} = \frac{\partial \vec{\mathbf{v}}}{\partial \vec{\mathbf{Y}}^T} \cdot \mathbf{C_Y} \cdot \frac{\partial \vec{\mathbf{v}}}{\partial \vec{\mathbf{Y}}^T} \tag{43}$$

The velocity vector is determined using six measurements, and the transformation relationship is:

$$\vec{\mathbf{v}} = \mathbf{M}_{\text{ECI}\leftarrow\hat{X}\hat{Y}\hat{Z}} \cdot \hat{\vec{\mathbf{v}}} \tag{44}$$

Because the matrix is relative to position measurements, the partial derivatives can be derived:

$$\frac{\partial \vec{\mathbf{v}}}{\partial \vec{\mathbf{Y}}^T} = \frac{\partial \mathbf{M}_{\text{ECI}\leftarrow\hat{X}\hat{Y}\hat{Z}}}{\partial \vec{\mathbf{Y}}^T} \cdot \hat{\vec{\mathbf{v}}} + \mathbf{M}_{\text{ECI}\leftarrow\hat{X}\hat{Y}\hat{Z}} \cdot \frac{\partial \hat{\vec{\mathbf{v}}}}{\partial \vec{\mathbf{Y}}^T} \tag{45}$$

Note that the matrix is determined only by the position measurements $\vec{\mathbf{Y}}_{\text{pos}}$. The partial derivatives of the matrix to kinematic measurements are 0, and that to position measurements is derived:

$$\frac{\partial \mathbf{M}_{\text{ECI}\leftarrow\hat{X}\hat{Y}\hat{Z}}}{\partial \vec{\mathbf{Y}}_{\text{pos}}^T} = \left[\frac{\partial \vec{\mathbf{e}}_{\hat{X}}}{\partial \vec{\mathbf{Y}}_{\text{pos}}^T} \frac{\partial \vec{\mathbf{e}}_{\hat{Y}}}{\partial \vec{\mathbf{Y}}_{\text{pos}}^T} \frac{\partial \vec{\mathbf{e}}_{\hat{Z}}}{\partial \vec{\mathbf{Y}}_{\text{pos}}^T}\right] \tag{46}$$

As the unit vectors of the three axes in the $\hat{X}\hat{Y}\hat{Z}$ coordinate system are provided in Equation (18), let $\overrightarrow{\mathbf{vec}}$ denote the vector $\frac{\vec{\rho}_{\text{r}}}{\rho_{\text{r}}} + \frac{\vec{\rho}_{\text{t}}}{\rho_{\text{t}}}$, the specific partial derivatives can be obtained as:

$$\begin{aligned}
\frac{\partial \vec{\mathbf{e}}_{\hat{Z}}}{\partial \vec{\mathbf{Y}}^T} &= \left(\frac{\mathbf{I}_{3\times 3}}{\left|\vec{\boldsymbol{\rho}}_{\text{t}} \times \vec{\boldsymbol{\rho}}_{\text{r}}\right|} - \frac{\left(\vec{\boldsymbol{\rho}}_{\text{t}} \times \vec{\boldsymbol{\rho}}_{\text{r}}\right) \cdot \left(\vec{\vec{R}} \times \vec{\boldsymbol{\rho}}_{\text{r}}\right)^T}{\left|\vec{\boldsymbol{\rho}}_{\text{t}} \times \vec{\boldsymbol{\rho}}_{\text{r}}\right|^3}\right) \cdot \frac{\partial\left(\vec{\boldsymbol{\rho}}_{\text{t}} \times \vec{\boldsymbol{\rho}}_{\text{r}}\right)}{\partial \vec{\mathbf{Y}}^T} \\
\frac{\partial \vec{\mathbf{e}}_{\hat{Y}}}{\partial \vec{\mathbf{Y}}^T} &= \left(\frac{\mathbf{I}_{3\times 3}}{\left|\overrightarrow{\mathbf{vec}}\right|} - \frac{\left(\overrightarrow{\mathbf{vec}}\right) \cdot \left(\overrightarrow{\mathbf{vec}}\right)^T}{\left|\overrightarrow{\mathbf{vec}}\right|^3}\right) \cdot \frac{\partial\left(\overrightarrow{\mathbf{vec}}\right)}{\partial \vec{\mathbf{Y}}^T} \\
\frac{\partial \vec{\mathbf{e}}_{\hat{X}}}{\partial \vec{\mathbf{Y}}^T} &= \frac{\partial\left(\vec{\mathbf{e}}_{\hat{Y}} \times \vec{\mathbf{e}}_{\hat{Z}}\right)}{\partial \vec{\mathbf{Y}}^T}
\end{aligned} \tag{47}$$

Because the position vector is known, the terms can be calculated by the derivation rule.

Consider the partial derivatives of the three velocity components in the $\hat{X}\hat{Y}\hat{Z}$ coordinate system. The derivative of $v_{\hat{y}}$ is simply calculated by Equation (23):

$$\frac{\partial v_{\hat{y}}}{\partial \vec{\mathbf{Y}}^T} = \left[\frac{\partial v_{\hat{y}}}{\partial \vec{\mathbf{Y}}_{\text{pos}}^T}, \frac{\partial v_{\hat{y}}}{\partial \dot{\rho}}\right] \tag{48}$$

The expressions of $v_{\hat{x}}$ and $v_{\hat{z}}$ are too complicated to directly analyze the partial derivations of measurements. Thus the binary system of equations composed of (30) and (32) is used. Taking the partial derivative of the two equations, two linear equations about $\frac{\partial v_{\hat{x}}}{\partial \vec{\mathbf{Y}}^T}$ and $\frac{\partial v_{\hat{z}}}{\partial \vec{\mathbf{Y}}^T}$ can be obtained:

$$\begin{cases} q_1 \dfrac{\partial v_{\hat{x}}}{\partial ob_i} + q_2 \dfrac{\partial v_{\hat{z}}}{\partial ob_i} + q_3 = 0 \\ p_1 \dfrac{\partial v_{\hat{x}}}{\partial ob_i} + p_2 \dfrac{\partial v_{\hat{z}}}{\partial ob_i} + p_3 = 0 \end{cases} \tag{49}$$

where ob_i is the ith element of $\vec{\mathbf{Y}}$ ($i = 1, \ldots, 6$). To simplify the expression, the coefficients of each term are substituted as follows:

$$\begin{aligned}
q_1 &= 2k_1 v_{\hat{x}} + k_2 \\
q_2 &= 2l_1 v_{\hat{z}} + l_2 \\
q_3 &= v_{\hat{x}}^2 \frac{\partial k_1}{\partial ob_i} + v_{\hat{x}} \frac{\partial k_2}{\partial ob_i} + v_{\hat{z}}^2 \frac{\partial l_1}{\partial ob_i} + v_{\hat{z}} \frac{\partial l_2}{\partial ob_i} + \frac{\partial m_1}{\partial ob_i} \\
p_1 &= 3c_1 v_{\hat{x}}^2 + 2c_2 v_{\hat{x}} + c_3 + c_4 v_{\hat{z}}^2 + c_8 v_{\hat{z}} \\
p_2 &= 2c_4 v_{\hat{x}} v_{\hat{z}} + 2c_5 v_{\hat{z}} + c_6 + c_8 v_{\hat{x}} \\
p_3 &= v_{\hat{x}}^3 \frac{\partial c_1}{\partial ob_i} + v_{\hat{x}}^2 \frac{\partial c_2}{\partial ob_i} + v_{\hat{x}} \frac{\partial c_3}{\partial ob_i} + v_{\hat{x}} v_{\hat{z}}^2 \frac{\partial c_4}{\partial ob_i} \\
&\quad + v_{\hat{z}}^2 \frac{\partial c_5}{\partial ob_i} + v_{\hat{z}} \frac{\partial c_6}{\partial ob_i} + \frac{\partial c_7}{\partial ob_i} + v_{\hat{x}} v_{\hat{z}} \frac{\partial c_8}{\partial ob_i}
\end{aligned} \tag{50}$$

Since the intermediate variables in the process of velocity determination are given, the coefficients can be obtained by using the chain rule. Then by solving Equation (49), the partial derivatives can be derived as:

$$\begin{aligned}
\frac{\partial v_{\hat{x}}}{\partial ob_i} &= \frac{p_3 q_2 - p_2 q_3}{p_2 q_1 - p_1 q_2} \\
\frac{\partial v_{\hat{z}}}{\partial ob_i} &= \frac{p_1 q_3 - p_3 q_1}{p_2 q_1 - p_1 q_2}
\end{aligned} \tag{51}$$

It is observed through simulations that the denominator of the partial derivative greatly affects the error of velocity determination. Define the singular discriminant $delta = p_2 q_1 - p_1 q_2$. When $delta$ equals 0, the performance of velocity determination is bad and this case is regarded as singular. Note that when the orbit plane is coincident with the bistatic plane, the variances $r_{\hat{z}}$ and $v_{\hat{z}}$ are equal to zero, which results in the infinitesimal coefficients of q_2 and p_2. Thus, the coplanar case is considered the known singular case. Now, by combining Equations (37) and (43), the VRMSE can be obtained.

In this section, the estimated orbital state dependence on the mesurements erorr is assessed. The error of the position determination is only related to the position measurements, while the error of the velocity determination is related to all the measurements including singular cases.

IV. SIMULATION RESULTS

To verify the performance of the proposed IOD method, some numerical simulations are provided in this section. Similar to the derivation of the method described in the former text, the J2 perturbations are neglected for simplification. The simulation scenarios are based on Low Earth Orbit (LEO) satellites. The orbital elements are shown in Table 1. Cases 1, 2, and 3 are used to simulate and verify the performance of typical LEO objects and there are no singular scenarios in these cases. Case 4 considers the orbit with a high Efficiency of 0.7, which is usually regarded as a highly elliptical orbit (HEO) object. Case 5 includes singular points in the velocity determination.

For each case, the extrapolation from the time is performed based on the two-body model. The extrapolation step length is set as 20s. Therefore, several observations along the whole passing arc are obtained. Each observation epoch is regarded as the short arc reference time, and then the measurement vector $\vec{\mathbf{Y}}$ for each observation can be derived from the observation equation. At each observation epoch, the IOD process is performed, and theoretical RMSEs are derived. The relative time between the observation epoch and the initial epoch is regarded as the reference in the figures. The locations of the two stations are shown in Table 2. The target is visible to both stations for all simulation scenarios.

In Section III, the RMSEs of the position and velocity vectors are derived, which represents the effect of the measurement error on the estimated state error. However, the procedure is based on a linearization approximation approach while the observation model is nonlinear. The model is approximately described using the first-order partial derivative of the state with respect to the observation. Monte Carlo experiments with 100,000 runs are performed to verify the

TABLE 1. Orbit parameters.

	a(km)	e	i(deg)	Ω(deg)	ν(deg)	ω(deg)
Case 1	7278.137	0.01	90	60	340	350
Case 2	7278.137	0.01	90	55	340	350
Case 3	7278.137	0.01	75	55	340	350
Case 4	25512.548	0.7	90	55	330	350
Case 5	7278.137	0.01	90	62	340	350

TABLE 2. Coordinate of observation stations.

	Longitude (deg)	Latitude (deg)	Height (m)
Receiving Station	60	0	150
Transmitting Station	70	0	0

reliability of the linearization. Each experiment can produce the deviations of position and velocity vectors, respectively, and the mean square error of these deviations can be approximated as the estimate error under the real observation model, as the number of experiments is large enough. In each figure, the legend 'MC' means the Monte Carlo simulation result, and the legend 'THEO' means the theoretical result.

TABLE 3. Parameters of observation stations.

Radar parameters	Value
Carrier Frequency	5.6 GHz
Signal Bandwidth	5 MHz
Integration Time	10 s
SNR	10 dB
Beam Width	1.2°

The radar parameters are provided in Table 3 for simulations. Then, the covariance matrices related to the parameters can be derived [24]:

$$\mathbf{C}_{position} = \begin{bmatrix} 1 & 0 & 0 \\ 0 & 1.44\text{E-}2 & 0 \\ 0 & 0 & 1.44\text{E-}2 \end{bmatrix}$$

$$\mathbf{C}_{doppler} = \begin{bmatrix} 6.806\text{E-}8 & 0 & -2.5\text{E-}7 \\ 0 & 6.533\text{E-}9 & 0 \\ -2.5\text{E-}7 & 0 & 9.147\text{E-}9 \end{bmatrix} \quad (52)$$

where the units of range and angle are square meters and square degrees. The units of velocity, acceleration, and jerk are square of meter per second (m^2/s^2), square of meter per second squared (m^2/s^4), and square of meter per second cubed (m^2/s^6), respectively.

A. PRMSE

As described in Equation (42), the PRMSE corresponds to the range error and two angle errors. Two observation cases are considered, one is that the target orbit passes over the receiving station right on the top, which means that the orbit coincides with the SZ plane, and the other is that the target passes over at a random angle. In cases 1 and 2, the position measurements and the PRMSE results are provided in Figures 4 and Figure 5, respectively.

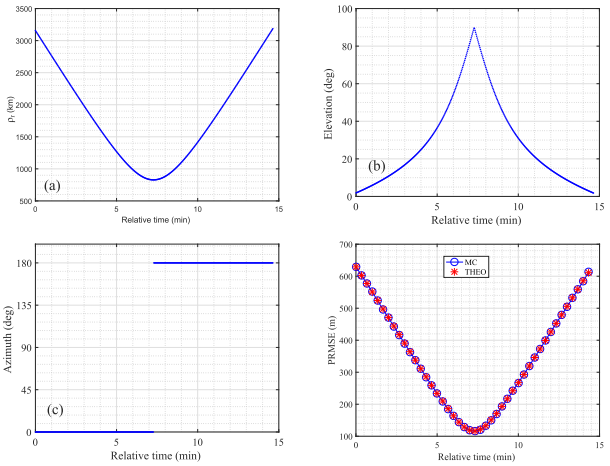

FIGURE 4. Case 1: (a) range. (b) elevation angle. (c) azimuth angle. (d) PRMSE.

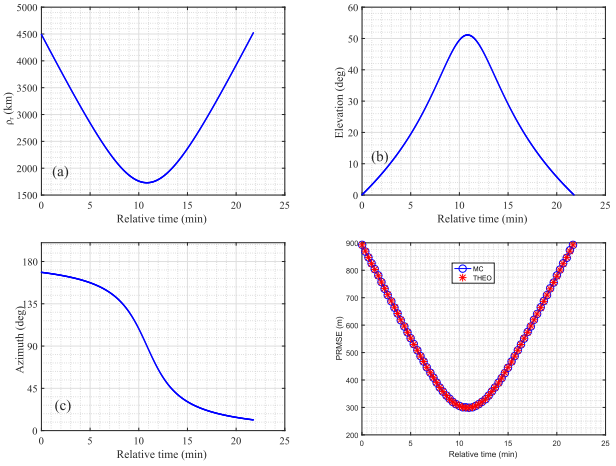

FIGURE 5. Case 2: (a) range. (b) elevation angle. (c) azimuth angle. (d) PRMSE.

The figures depict that the theoretical PRMSE is consistent with the Monte Carlo results. Analyzing the magnitude of each item of PRMSE in Equation (42) and comparing with the simulation results, it can be found that the PRMSE is mainly affected by ρ_r and el. For a single pass, when the elevation reaches the maximum and the range ρ_r reaches the minimum, the PRMSE is attained. We conclude that the best performance of position determination appears when the target passes over the receiving station.

B. VRMSE

Since the velocity determination does not have a simple analytical expression and is derived from a quartic equation, the performance analysis is complicated. After simplifying the covariance matrix in Equation (43), it is influenced by many factors including position geometry and velocity components. Simulations of different aspects are considered. First, two non-singular observation cases are considered, and

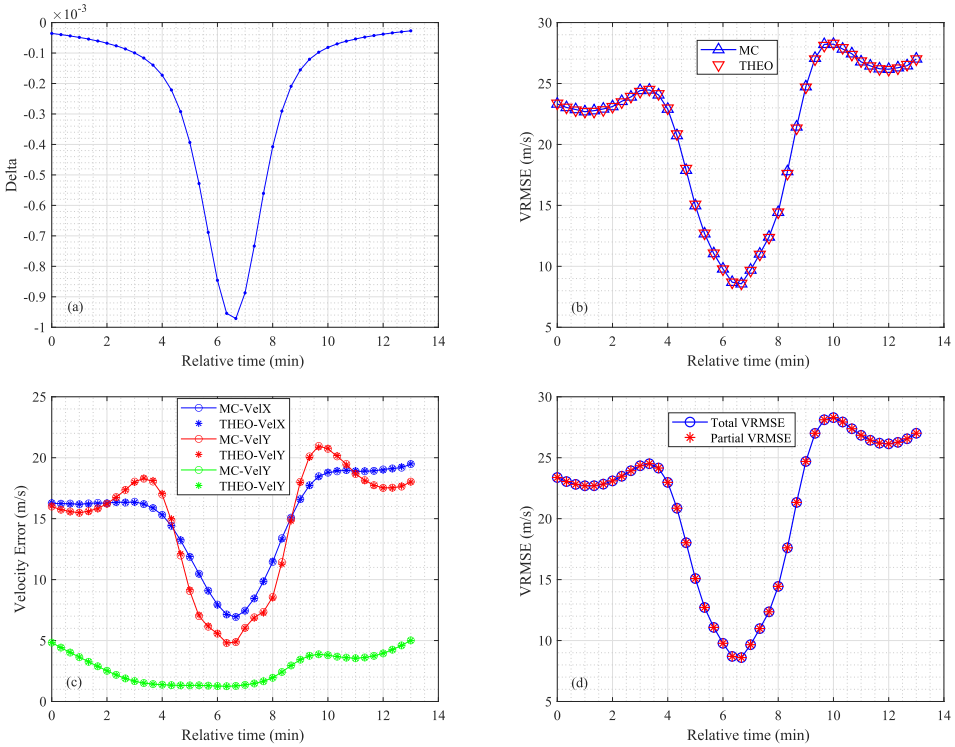

FIGURE 6. Case 2: (a) *delta*. (b) VRMSE. (c) errors of velocity components. (d) partial VRMSE.

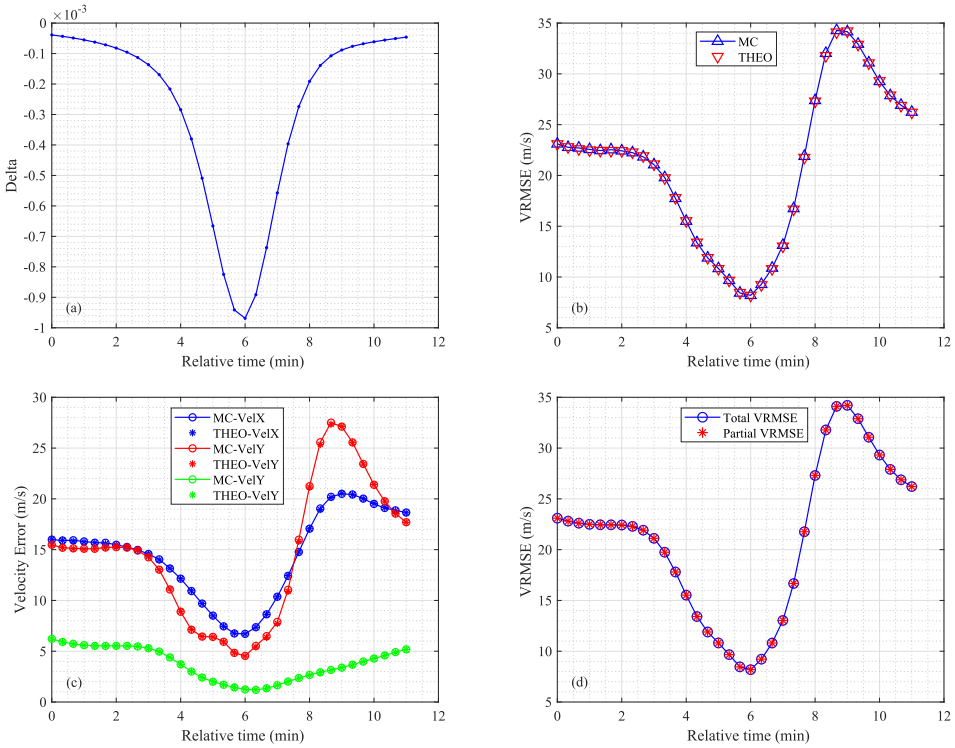

FIGURE 7. Case 3: (a) *delta*. (b) VRMSE. (c) errors of velocity components. (d) partial VRMSE.

theoretical results with Monte Carlo results are compared. Then, as mentioned before, the denominator of partial derivatives in Equation (51) would cause singular cases when it nearly equals 0. Simulations are carried out for this case. Finally, by traversing the ascending node and changing the orbit inclination, and in all visible arcs, a contour map of the

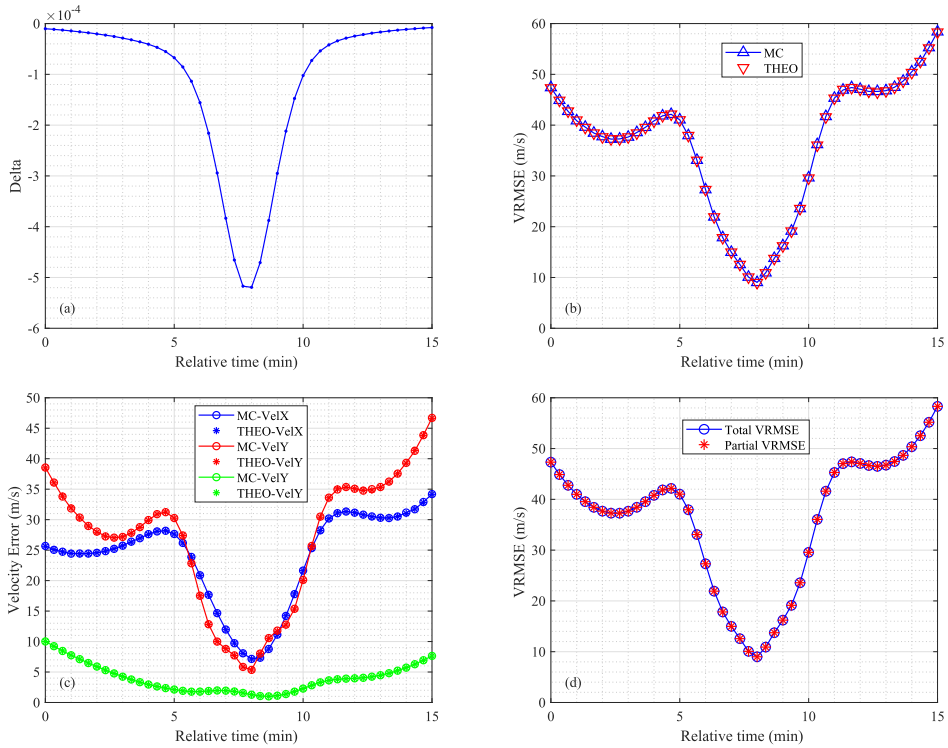

FIGURE 8. Case 4: (a) *delta*. (b) VRMSE. (c) errors of velocity components. (d) partial VRMSE.

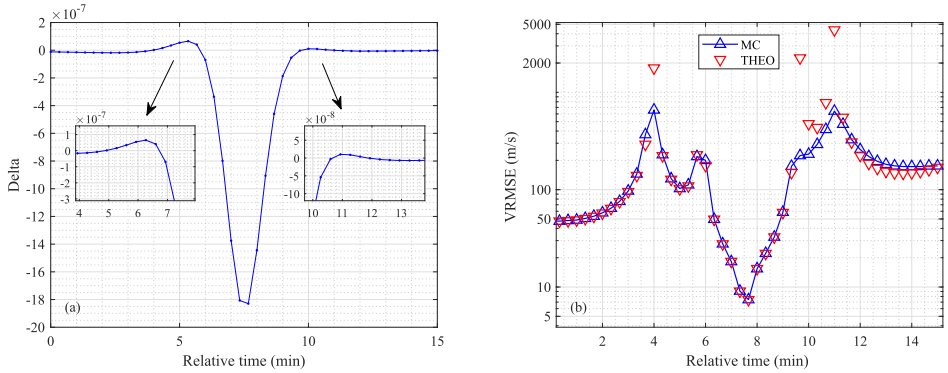

FIGURE 9. Case 5: (a) *delta*. (b) VRMSE.

velocity error is provided as a reference to choose the better observation scenarios.

1) NONSINGULAR CASES

The two cases 2 and 3 have different inclinations of 90° and 75°, and the ascending node is set at 55°. Case 4 is the orbit with high eccentricity. The results are shown in Figures 6, 7, and 8, where the subfigures have the following representations: (a) As the sign to judge singular cases, the denominator in Equation (51) is given, which is denoted as *delta*; (b) the comparison between theoretical VRMSE and Monte Carlo VRMSE is done; (c) The errors of velocity components in ECI system are provided; (d) the comparison between theoretical total VRMSE and the partial VRMSE, when the measurements are only perturbed by the jerk and angle errors, is provided.

As depicted in Figs. (a), the arcs have no cases in which *delta* equals 0. Obviously, the error is inversely proportional to the absolute value of *delta*. Figs. (b) depict that the theoretical VRMSE values are consistent with the Monte Carlo results. Note that the minimum VRMSE appears when the target nearly passes over the receiving station, and the VRMSE can reach several meters per second when the elevation angle is larger than 25°. Combined with the analysis in PRMSE, it shows that the best performance of the proposed IOD method appears when the elevation angle reaches the largest value for a nonsingular pass. The results shown in Figs. (c) demonstrate that the linearization approximation is

reliable. The velocity error components in the three directions of the ECI system are consistent with the simulations. Experiments show that the total VRMSE is mainly influenced by the partial derivative of the estimated velocity with respect to the jerk and the angles. Therefore, the comparison is provided in Figs. (d). It has been verified that for the whole arc, this partial VRMSE value is almost the same as the total VRMSE value, which means that the error of velocity determination is determined by the three measurements: *az*, *el*, and jerk.

2) SINGULAR CASES

An arc with the singular observation scenario, regarded as case 5, is used for simulation, where the discriminant *delta* has zero points. The orbit inclination is 90° and the ascending node is 62°. As shown in Figure 9(a), *delta* has four zero points. Since the denominator equal to zero makes no practical sense, the near-zero interval is observed. Figure 9(b) depicts the results of VRMSE containing singular cases. When *delta* is nearly 0 points, the nonlinear effects cannot be ignored. Although the two results are not consistent, the Monte Carlo results show that the proposed solution of velocity does have poor performance when delta equals 0, and the lowest accuracy of velocity determination could reach kilometers per second. This is intolerable for the absolute velocity of LEO targets. Therefore, in actual scenarios, a larger absolute magnitude discriminant *delta* is the premise for better IOD accuracy.

3) SCENARIO TRAVERSAL

The discriminant *delta* has a great influence on the VRMSE and is jointly determined by the target position and velocity. Simulations for some common scenarios are carried out to help avoid singular cases. By traversing the ascending node, the target appears at the position in the entire visible range. By changing the orbit inclination, the effect of different velocity directions on the VRMSE can also be represented.

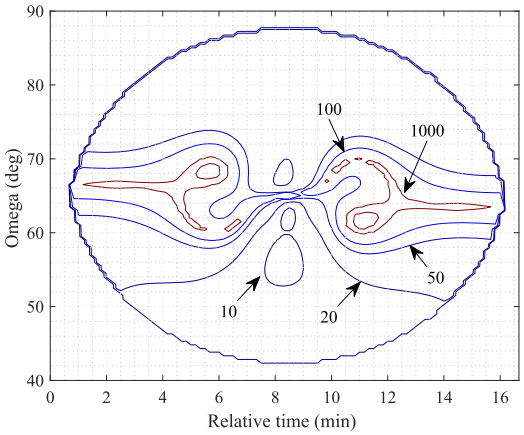

FIGURE 10. VRMSE of scenario traversal with 90° orbital inclination.

The first cases have a constant orbit inclination of 90°, and the results are shown in Figure 10. The relationship between the VRMSE and the ascending node Omega is provided. The numbers indicated in the figure are VRMSE contours, where the unit is meters per second. The outermost line distinguishes the visibility. Because the station longitudes are 60° and 70°, the traversal range of Omega is from 40° to 70°. The second cases have a constant orbit inclination of 75° and are shown in Figure 11. The outermost line is at an angle to the central axis, and the whole graph is symmetric about the center point. The largest VRMSE, which reaches kilometers per second, appears when the target is nearly located in the plane, about which the two station positions are symmetric. The best VRMSE appears when the target passes over the top of one station and can reach several meters per second. As a consequence, for a single pass, the optimal observation scenario, in which the error of the IOD method can satisfy the needs for the initial orbit, is when the target passes over the top of stations, and the target is not located near the central vertical plane of the two-station baseline.

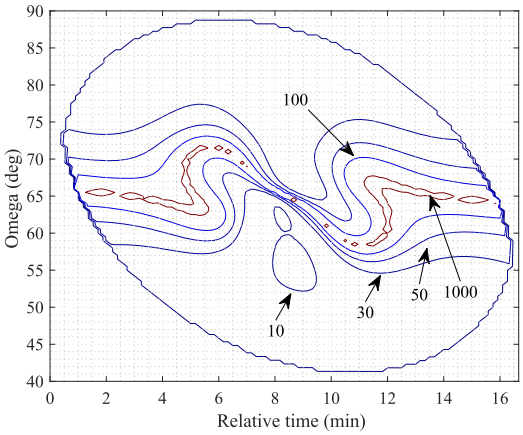

FIGURE 11. VRMSE of scenario traversal with 75° orbital inclination.

V. CONCLUSION

In this paper, we present a new initial orbit determination method using a single too-short-arc observation based on bistatic radar. By using measurements including the bistatic range, azimuth and elevation angles, the bistatic velocity, acceleration, and jerk, a closed-form solution for the space object state is derived, which contains the position and velocity vectors. As the relationship between the state and the bistatic high order kinematic measurements is more complex than that of a monostatic radar, the undetermined parameters are coupling in the observation equations. By defining an auxiliary coordinate system based on bistatic geometry, the parameters are separated and the equations are transformed into a binary system that the analytical solution can be derived. Finally, we use coordinate transformations to obtain the closed-form expressions of the orbital state. We evaluate the performance of the proposed method by RMSE, and the position and velocity errors are represented by the linearization approach. Simulations for theoretical and Monte Carlo results are performed for verification. Additionally, the singular cases with poor IOD performance are considered,

where the errors are not acceptable for normal LEO objects. To avoid singular cases, simulations of some LEO scenarios are provided as a reference for better IOD performance.

The method uses the measurements obtained from a single too-short arc observation to derive the complete orbital state vector. No additional information or multiple observations are required. The process provides the setup for new detected targets that must be catalogued by the space surveillance system. When more observations are gathered, the data association or precise orbit determination can be performed based on the derived initial orbit.

APPENDIX A

For simplifying the expression in Equation (26), the specifitic substitutions are provided as follows:

$$k_{r1} = \frac{y_r^2}{\rho_r^3}, k_{r2} = -\frac{2x_r y_r v_{\hat{y}}}{\rho_r^3} - \frac{2v_{rx}}{\rho_r} + \frac{2x_r\left(\dot{\hat{\boldsymbol{\rho}}}_r \cdot \dot{\hat{\mathbf{S}}}_r\right)}{\rho_r^3} \tag{53}$$

$$l_{r1} = \frac{1}{\rho_r}, l_{r2} = -\frac{2v_{rz}}{\rho_r} \tag{54}$$

$$m_r = \frac{1}{\rho_r}\left(v_{\hat{y}}^2 + \left|\dot{\hat{\mathbf{S}}}_r\right|^2 - 2v_{ry}v_{\hat{y}}\right) - \frac{1}{\rho_r^3}\left(y_r v_{\hat{y}} - \left(\hat{\boldsymbol{\rho}}_r \cdot \dot{\hat{\mathbf{S}}}_r\right)\right)^2 + \frac{\vec{\boldsymbol{\rho}}_r\left(\ddot{\vec{\mathbf{r}}} - \ddot{\vec{\mathbf{S}}}_r\right)}{\rho_r} \tag{55}$$

$$k_{t1} = \frac{y_t^2}{\rho_t^3}, k_{t2} = -\frac{2x_t y_t v_{\hat{y}}}{\rho_t^3} - \frac{2v_{tx}}{\rho_t} + \frac{2x_t\left(\dot{\hat{\boldsymbol{\rho}}}_t \cdot \dot{\hat{\mathbf{S}}}_t\right)}{\rho_t^3} \tag{56}$$

$$l_{t1} = \frac{1}{\rho_t}, l_{t2} = -\frac{2v_{tz}}{\rho_t} \tag{57}$$

$$m_t = \frac{1}{\rho_t}\left(v_{\hat{y}}^2 + \left|\dot{\hat{\mathbf{S}}}_t\right|^2 - 2v_{ty}v_{\hat{y}}\right) - \frac{1}{\rho_t^3}\left(y_t v_{\hat{y}} - \left(\hat{\boldsymbol{\rho}}_t \cdot \dot{\hat{\mathbf{S}}}_t\right)\right)^2 + \frac{\vec{\boldsymbol{\rho}}_t\left(\ddot{\vec{\mathbf{r}}} - \ddot{\vec{\mathbf{S}}}_t\right)}{\rho_t} \tag{58}$$

For simplifying the expression in Equation (32), the details of the variable substitution are provided in the text:

$$c_1 = -\frac{3x_r k_{r1}}{\rho_r^2} - \frac{3x_t k_{t1}}{\rho_t^2} \tag{59}$$

$$c_2 = -\frac{3x_r k_{r2} + 3y_r k_{r1} v_{\hat{y}}}{\rho_r^2} - \frac{3x_t k_{t2} + 3y_t k_{t1} v_{\hat{y}}}{\rho_t^2} + \frac{3\vec{\boldsymbol{\rho}}_r \cdot \dot{\vec{\mathbf{S}}}_r}{\rho_r^2} k_{r1} + \frac{3\vec{\boldsymbol{\rho}}_t \cdot \dot{\vec{\mathbf{S}}}_t}{\rho_t^2} k_{t1} \tag{60}$$

$$c_3 = -\frac{3x_r m_r + 3y_r k_{r2} v_{\hat{y}} - 3k_{r2}\vec{\boldsymbol{\rho}}_r \cdot \dot{\vec{\mathbf{S}}}_r + 3\rho_r a_{rx}}{\rho_r^2} - \frac{3x_t m_t + 3y_t k_{t2} v_{\hat{y}} - 3k_{t2}\vec{\boldsymbol{\rho}}_t \cdot \dot{\vec{\mathbf{S}}}_t + 3\rho_t a_{tx}}{\rho_t^2} + n r_{\hat{x}} \tag{61}$$

where $\ddot{\hat{\mathbf{S}}}_r = \left[a_{rx}, a_{ry}, a_{rz}\right]^T$ and $\ddot{\hat{\mathbf{S}}}_t = \left[a_{tx}, a_{ty}, a_{tz}\right]^T$ are the coordinates of station accelerations in the $\hat{X}\hat{Y}\hat{Z}$ system.

$$c_4 = -\frac{3x_r}{\rho_r^3} - \frac{3x_t}{\rho_t^3} \tag{62}$$

$$c_5 = -\frac{3y_r v_{\hat{y}} - 3\vec{\boldsymbol{\rho}}_r \cdot \dot{\vec{\mathbf{S}}}_r}{\rho_r^3} - \frac{3y_t v_{\hat{y}} - 3\vec{\boldsymbol{\rho}}_t \cdot \dot{\vec{\mathbf{S}}}_t}{\rho_t^3} \tag{63}$$

$$c_6 = -3l_{r2}\frac{y_r v_{\hat{y}} - \vec{\boldsymbol{\rho}}_r \cdot \dot{\vec{\mathbf{S}}}_r}{\rho_r^2} - 3l_{t2}\frac{y_t v_{\hat{y}} - \vec{\boldsymbol{\rho}}_t \cdot \dot{\vec{\mathbf{S}}}_t}{\rho_t^2} + n r_{\hat{z}} - 3\left(\frac{a_{rz}}{\rho_r} + \frac{a_{tz}}{\rho_t}\right) \tag{64}$$

$$c_7 = -3m_r\frac{y_r v_{\hat{y}} - \vec{\boldsymbol{\rho}}_r \cdot \dot{\vec{\mathbf{S}}}_r}{\rho_r^2} - 3m_t\frac{y_t v_{\hat{y}} - \vec{\boldsymbol{\rho}}_t \cdot \dot{\vec{\mathbf{S}}}_t}{\rho_t^2} - \frac{\mu}{r^3}\dot{\rho} + n r_{\hat{y}} v_{\hat{y}} - 3\left(\frac{a_{ry}}{\rho_r} + \frac{a_{ty}}{\rho_t}\right) v_{\hat{y}} - \frac{\mu}{r^3}\left(\frac{\vec{\boldsymbol{\rho}}_r \cdot \dot{\vec{\mathbf{S}}}_r}{\rho_r} + \frac{\vec{\boldsymbol{\rho}}_t \cdot \dot{\vec{\mathbf{S}}}_t}{\rho_t}\right) + 3\frac{\mu}{r^3}\left(\frac{\vec{\mathbf{r}} \cdot \dot{\vec{\mathbf{S}}}_r}{\rho_r} + \frac{\vec{\mathbf{r}} \cdot \dot{\vec{\mathbf{S}}}_t}{\rho_t}\right) \tag{65}$$

$$- \left(\frac{\vec{\boldsymbol{\rho}}_r \cdot \dddot{\vec{\mathbf{S}}}_r}{\rho_r} + \frac{\vec{\boldsymbol{\rho}}_t \cdot \dddot{\vec{\mathbf{S}}}_t}{\rho_t}\right) \tag{66}$$

$$c_8 = -3\left(\frac{x_r l_{r2}}{\rho_r} + \frac{x_t l_{t2}}{\rho_t}\right)$$

$$n = -3\left(\frac{\mu\left(\vec{\mathbf{r}} \cdot \vec{\mathbf{S}}_r\right)}{\rho_r r^5} + \frac{\mu\left(\vec{\mathbf{r}} \cdot \vec{\mathbf{S}}_t\right)}{\rho_t r^5}\right) \tag{67}$$

And the further substitutions from (32) to (33) are:

$$c_3' = c_3 - \frac{l_2}{2l_1}c_8 + \frac{l_2^2}{4l_1^2}c_4 \tag{68a}$$

$$c_6' = c_6 - \frac{l_2}{l_1}c_5 \tag{68b}$$

$$c_7' = \frac{l_2^2}{4l_1^2}c_5 - \frac{l_2}{2l_1}c_6 + c_7 \tag{68c}$$

$$c_8' = c_8 - \frac{l_2}{l_1}c_4 \tag{68d}$$

Let $m_2 = m_1' - \ddot{\rho}$, the substitution in (35) are provided:

$$f_1 = \left(c_2 - \frac{c_4 k_2}{l_1} - \frac{c_5 k_1}{l_1}\right)^2 + \frac{c_8'^2 k_1}{l_1} \tag{69}$$

$$f_2 = 2\left(c_2 - \frac{c_4 k_2}{l_1} - \frac{c_5 k_1}{l_1}\right)\left(c_3' - \frac{c_4 m_2}{l_1} - \frac{c_5 k_2}{l_1}\right) + \frac{c_8'^2 k_2}{l_1} + \frac{2c_6' c_8' k_1}{l_1} \tag{70}$$

$$f_3 = \left(c_3' - \frac{c_4 m_2}{l_1} - \frac{c_5 k_2}{l_1}\right)^2 + 2\left(c_2 - \frac{c_4 k_2}{l_1} - \frac{c_5 k_1}{l_1}\right)\left(c_7' - \frac{c_5 m_2}{l_1}\right)$$

$$+\frac{c'^2_6 k_1 + +2c'_6 c'_8 k_2 + c'^2_8 m_2}{l_1} \tag{71}$$

$$f_4 = 2\left(c'_3 - \frac{c_4 m_2}{l_1} - \frac{c_5 k_2}{l_1}\right)\left(c'_7 - \frac{c_5 m_2}{l_1}\right) + \frac{c'^2_6 k_2 + 2c'_6 c'_8 m_2}{l_1} \tag{72}$$

$$f_5 = \left(c'_7 - \frac{c_5 m_2}{l_1}\right)^2 + c'^2_6 \frac{m_2}{l_1} \tag{73}$$

APPENDIX B

There are methods to solve the quartic equations, and we provide the procedure of Ferrari's solution for finding $v_{\hat{x}}$ in Equation (35). Given a general form of a quartic equation as

$$ax^4 + bx^3 + cx^2 + dx + e = 0 \tag{74}$$

We can get the roots following this process:

$$\begin{aligned}
P &= \frac{c^2 + 12ae - 3bd}{9} \\
Q &= \frac{27ad^2 + 2c^3 + 27b^2 e - 72ace - 9bcd}{54} \\
D &= \sqrt{Q^2 - P^3} \\
u &= \begin{cases} \sqrt[3]{Q+D}, & \left|\sqrt[3]{Q+D}\right| \geq \left|\sqrt[3]{Q-D}\right| \\ \sqrt[3]{Q-D}, & \left|\sqrt[3]{Q+D}\right| < \left|\sqrt[3]{Q-D}\right| \end{cases} \\
v &= \frac{P}{u} \\
w &= -\frac{1}{2} + \frac{\sqrt{3}}{2} i \\
m &= \sqrt{b^2 - \frac{8}{3}ac + 4a\left(w^{k-1}u + w^{4-k}v\right)}, (k = 1, 2, 3) \\
&= \sqrt{b^2 - \frac{8}{3}ac + 4a\left(u + v\right)}, (k = 1, when\ |m| \neq 0) \\
S &= 2b^2 - \frac{16}{3}ac - 4a\left(w^{k-1}u + w^{4-k}v\right), (k = 1, 2, 3) \\
&= 2b^2 - \frac{16}{3}ac - 4a\left(u + v\right), (k = 1) \\
T &= \frac{8abc - 16a^2 d - 2b^3}{m} \\
x_n &= \frac{-b + (-1)^{\lceil n/2 \rceil} m + (-1)^{n+1} \sqrt{S + (-1)^{\lceil n/2 \rceil} T}}{4a}
\end{aligned} \tag{75}$$

The subscript n represents the nth root of the equation, and $v_{\hat{x}}$ can be obtained for further velocity determination.

REFERENCES

[1] J.-C. Liou and N. L. Johnson, "Risks in space from orbiting debris," *Science*, vol. 311, pp. 340–341, Jan. 2006.
[2] E. Olmedo, N. Sánchez-Ortiz, M. R. Lerate, M. Belló-Mora, H. Klinkrad, and F. Pina, "Initial orbit determination algorithms for cataloguing optical measurements of space debris," *Monthly Notices Roy. Astronomical Soc.*, vol. 391, no. 3, pp. 1259–1272, Dec. 2008.
[3] J. O. Cappellari, "Mathematical theory of the Goddard trajectory determination system," NASA STI, Recon Tech. Rep. N, 1976.
[4] S. Alinder, "Space situational awareness with the Swedish Allsky meteor network," Uppsala Univ., 1976.
[5] P. R. Escobal, *Methods of Orbit Determination*. New York, NY, USA: Wiley, 1965.
[6] A. Milani, G. F. Gronchi, M. D. M. Vitturi, and Z. Knežević, "Orbit determination with very short arcs. I admissible regions," *Celestial Mech. Dyn. Astron.*, vol. 90, nos. 1–2, pp. 57–85, Sep. 2004.
[7] A. Milani, G. Gronchi, Z. Knezevic, M. Sansaturio, and O. Arratia, "Orbit determination with very short arcs: II. Identifications," *Icarus*, vol. 179, no. 2, pp. 350–374, Dec. 2005.
[8] K. J. DeMars, M. K. Jah, and P. W. Schumacher, "Initial orbit determination using short-arc angle and angle rate data," *IEEE Trans. Aerosp. Electron. Syst.*, vol. 48, no. 3, pp. 2628–2637, Jul. 2012.
[9] K. J. DeMars and M. K. Jah, "Probabilistic initial orbit determination using Gaussian mixture models," *J. Guid., Control, Dyn.*, vol. 36, no. 5, pp. 1324–1335, Sep. 2013.
[10] L. Ansalone and F. Curti, "A genetic algorithm for initial orbit determination from a too short arc optical observation," *Adv. Space Res.*, vol. 52, no. 3, pp. 477–489, Aug. 2013.
[11] H. Hinagawa, H. Yamaoka, and T. Hanada, "Orbit determination by genetic algorithm and application to GEO observation," *Adv. Space Res.*, vol. 53, no. 3, pp. 532–542, Feb. 2014.
[12] H. R. Battin, "An introduction to the mathematics and methods of astrodynamics, revised edition," Amer. Inst. Aeronaut. Astronaut., Reston, VA, USA, 1999.
[13] D. Izzo, "Revisiting Lambert's problem," *Celestial Mech. Dyn. Astron.* vol. 121, pp. 1–15, Oct. 2015.
[14] R. H. Gooding, "A procedure for the solution of Lambert's orbital boundary-value problem," *Celestial Mech. Dyn. Astron.* vol. 48, pp. 145–165, Jun. 1990.
[15] G. Tommei, A. Milani, and A. Rossi, "Orbit determination of space debris: Admissible regions," *Celestial Mech. Dyn. Astron.*, vol. 97, no. 4, pp. 289–304, 2007.
[16] K. J. DeMars and M. K. Jah, "Probabilistic initial orbit determination using radar returns," in *Proc. AAS/AIAA Astrodyn. Spec. Conf.*, Hilton Head, SC, USA, vol. 150, 2014, pp. 35–54.
[17] M. L. Smith, "Tristatic tracking filter used by the multistatic measurement system," MIT Lincoln Lab., Lexington, KY, USA, Tech. Rep. 699, 1984.
[18] T. J. Abatzoglou and G. O. Gheen, "Range, radial velocity, and acceleration MLE using radar LFM pulse train," *IEEE Trans. Aerosp. Electron. Syst.*, vol. 34, no. 4, pp. 1070–1083, Oct. 1998.
[19] H. Shang, D. Chen, H. Cao, T. Fu, and M. Gao, "Initial orbit determination using very short arc data based on double-station observation," *IEEE Trans. Aerosp. Electron. Syst.*, vol. 55, no. 4, pp. 1596–1611, Aug. 2019.
[20] S. Zhang, T. Fu, D. Chen, S. Ding, and M. Gao, "An initial orbit determination method using single-site very short arc radar observations," *IEEE Trans. Aerosp. Electron. Syst.*, vol. 56, no. 3, pp. 1856–1872, Jun. 2020.
[21] N. J. Willis, *Bistatic Radar*. Raleigh, NC, USA: SciTech Publishing, 2005, ch. 1, pp. 1–7.
[22] N. J. Willis and H. D. Griffiths, *Advances in Bistatic radar*. Raleigh, NC, USA: SciTech Publishing, 2007.
[23] D. A. Vallado and W. D. McClain, *Fundamentals of Astrodynamics and Applications* (Space Technology Series). New York, NY, USA: McGraw-Hill, 1997, pp. 31–55.
[24] S. Ding, D. Chen, H. Cao, and T. Fu, "Exact and closed-form CRLBS for high-order kinematic parameters estimation using LFM coherent pulse train," *IEEE Access*, vol. 6, pp. 57447–57459, 2018.
[25] S. M. Kay, *Fundamentals of Statistical Signal Processing*, vol. 1. Englewood Cliffs, NJ, USA: Prentice-Hall, 1993.

JINYE QU received the B.S. degree in electronic engineering from the Beijing Institute of Technology, China, in 2015, where he is currently pursuing the Ph.D. degree in information and communication engineering. His research interests include radar system analysis, space target orbit determination, and parameter estimation techniques.

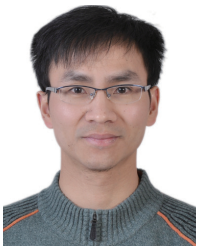

DEFENG CHEN was born in Longyan, Fujian, China, in 1983. He received the B.S. and Ph.D. degrees in electronic engineering from the Beijing Institute of Technology, China, in 2006 and 2011, respectively. He is currently an Associate Researcher with the School of Information and Electronics, Beijing Institute of Technology. His research interests include radar signal processing and its applications in space target detection.

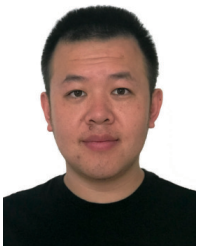

HUAWEI CAO received the B.S. degree in electronic science and technology from Yanshan University, China, in 2009, and the Ph.D. degree in electronic engineering from the Beijing Institute of Technology, China, in 2016. He is currently a Lecturer with the School of Information and Electronics, Beijing Institute of Technology. His research interests include radar system analysis and long-time coherent integration techniques for weak target detection.

TUO FU was born in Shenyang, Liaoning, China, in 1977. He received the Ph.D. degree in electronic engineering from the Beijing Institute of Technology, China, in 2004. From 2004 to 2006, he was a Postdoctoral Researcher with the National Mobile Communications Research Laboratory, Southeast University, China. Since 2006, he has been a Researcher with the School of Information and Electronics, Beijing Institute of Technology. His research interests include radar system design and statistical signal processing.

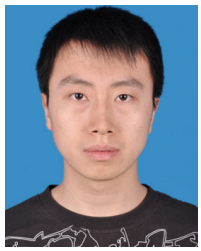

SHUO ZHANG was born in Baoding, Hebei, China, in 1992. He received the B.S. degree in electronic science and technology from Yanshan University, China, in 2014, and the Ph.D. degree in electronic engineering from the Beijing Institute of Technology, China, in 2021, respectively. He is currently a Postdoctoral Researcher with the School of Information and Electronics, Beijing Institute of Technology. His research interests include space situational awareness and statistical signal processing.